(DOI: will be inserted by hand later)

Interferometric Remapped Array Nulling

F. Vakili[1], E. Aristidi[1], L. Abe[1], and B. Lopez[2]

[1] Laboratoire Univ. d'Astroph. de Nice (LUAN), CNRS UMR 6525, Parc Valrose, 06108 Nice Cedex 02, France

[2] Laboratoire Fresnel, CNRS UMR 6528, Observatoire de la Côte d'Azur, B.P. 4229, 06304 Nice cedex 4

Received xx/xx/01 / Accepted yy/yy/01

Abstract. This paper describes a method of beam-combination in the so-called hypertelescope imaging technique recently introduced by Labeyrie in optical interferometry. The method we propose is an alternative to the Michelson pupil reconfiguration that suffers from the loss of the classical object-image convolution relation. From elementary theory of Fourier optics we demonstrate that this problem can be solved by reconfiguring images instead of pupils. Imaging is performed in a combined pupil-plane where the point-spread function (PSF) tends towards a pseudo Airy disc for a sufficiently large number of telescopes. Our method is applicable to snap-shot imaging of extended sources with a field limited to the Airy pattern of single telescopes operated in a co-phased multi-aperture interferometric array. It thus allows to apply conveniently focal plane coronagraphy. Our technique called Interferometric Remapped Array Nulling (IRAN) is particularly suitable for high dynamic imaging of extra-solar planetary companions or extra-galactic objects where long baseline interferometry would closely probe the central regions of AGNs for instance. We also discuss the application of IRAN to improve the performances of imaging and/or nulling interferometers like the full-fledged VLTI array or the DARWIN space-borne mission.

Key words. Techniques:high angular resolution – Techniques:interferometry – Techniques:imaging

1. Introduction

Modern optical interferometry is among the most promising techniques to directly detect and characterize extra-solar planets (ExPN) using the so-called nulling (Bracewell, 1978)

Send offprint requests to: Farrokh Vakili,e-mail: `Farrokh.Vakili@unice.fr`

or differential interferometry (Petrov et al., 2000). Nulling means to reject the light of the on-axis star to detect its ExPN otherwise enshrouded by the star diffracted light. The technique is now being effectively considered on large telescope ground-based arrays like the VLTI-GENIE (Gondoin et al., 2003) among others or space-borne missions such as DARWIN (Mennesson & Mariotti, 1997) or TPF (Beichman, et al., 2002). Quite recently, alternative techniques such as apodized apertures (Soummer et al., 2003, Gonsalves & Nisenson, 2003) or coronagraphic densified arrays of telescopes, also called hypertelescopes (Labeyrie et al., 2003), have been proposed to achieve the same goal with the bonus of offering imaging possibilities up to the diffraction limit set by their baseline.

Compared to Bracewell nulling interferometry, the concept of densified pupil-hypertelescope presents in principle the additional advantage of separating the ExPN energy from the emission of its parent star. Therefore and compared to the co-axial combination considered by nulling interferometers, densified-pupil hypertelescopes should be more immune from the exo-zodiacal contamination inherent to co-axial pupil-plane detection techniques used for DARWIN or TPF missions. On the other hand, in a densified-pupil the basic relation of image formation from the convolution of the PSF to sky brightness degrades as a function of input versus output baselines normalized to the geometric telescope size. Thus the non-aberrated imaging field of view of a hypertelescope can dramatically decrease with increasing densification factor γ (Gillet et al., 2003) which is a generalization of the classical Michelson periscopic set-up for stellar interferometry (Michelson, 1920). As already noted by Labeyrie and in absence of optical aberrations this field, also called Zero-Order-Field (ZOF), becomes intrinsically small and attains a small fraction of the primary field of the elementary telescopes that form the interferometric array. In addition, the image of any off-axis object, an ExPN for instance, is spectrally dispersed in the radial direction from the center of the field as a function of its distance to that center. The advantage of a densified optical array of telescopes equipped by an image-plane phase coronagraph over a nulling long baseline interferometer remains an open question that several groups are studying both for theoretical and laboratory prototyping aspects.

In the followings we propose a pupil-plane imaging technique which is strictly equivalent to the hypertelescope technique. However it has the great advantage to conserve the convolution relation of image formation limited to the Airy figure of primary telescopes. We first schematically describe the principle of our technique called Interferometric Remapped-Array Nulling (IRAN), establish formally its operation and describe its various properties through numerical simulations. Two different optical set-ups to practically implement the IRAN technique making use of a phase masked coronagraph for ExPN detection are also outlined and finally the application of IRAN to ground-based as well as space-borne missions is discussed.

2. Principle of IRAN

Labeyrie's hypertelescope concept is based on densifying the output pupil of an interferometric array by conserving the primary telescope orientations respective to each other to form the equivalent of a single dish telescope with a continuous surface. This is obtained for instance by re-imaging the output pupils on a pyramidal beam combiner (Gillet et al., 2003). The resulting diffraction pattern obtained from the pseudo-single densified aperture will correspond to an Airy pattern if the sub-apertures were to be co-phased, thus resembling to a monolithic giant dish Airy pattern. In the IRAN concept beam-combination is simply obtained by forming output images from primary telescopes on the same pyramid as for the hypertelescope (Fig. 1). A relay lens is then used to stack all the output pupils on the top of each other and record their interference on a 2D detector.

2.1. Technical implementation

To better understand the operating principle of IRAN it is useful to recall the academic Fizeau versus Michelson optical set-ups for stellar interferometry. In a Fizeau-type beam combination (Fig. 1A) the light beams from segments of a giant primary mirror are focused by a secondary Cassegrain mirror to form a fringe pattern which modulates the refolded Airy discs. Both these patterns undergo the same angular magnification which depends on the mirror segments size and their spacing. In general the more distant the segments the more fringes across the Airy pattern. On the contrary in the Michelson set-up (Fig. 1B) the fringe modulation does not depend on the spacing between the input telescope pupil size but on the output pupils as seen from the focal superimposed Airy patterns. In the Michelson set-up the basic convolution relation between the Point Spread Function and the object intensity distribution on the sky is lost making image reconstruction from the measure of the complex visibility function mandatory. In both cases the fringe intensity pattern is modulated by the Airy envelope. The Michelson set-up can be further modified (Chelli & Mariotti, 1986) to form the Airy discs on the faces of the beam-combination mirror followed by a relay lens (Fig. 1C) which would form two superimposed and cosine-modulated output pupils where the fringe period depends on the Airy disc pattern distance as seen from the two superimposed pupils. In this case the fringe modulation remains constant across the support of the superimposed pupils. Now if much more than 2 Airy patterns were remapped from a large number of input mirror segments the different period and orientation of the resulting cosine fringe modulations will produce a central bright spot at the center of the conjugate stacked pupil for an on-axis star.

Two beam-combination schemes could be envisaged in this case: a classical bulky optical pyramidal shape mirror (Rousselet-Perraut et al., 1997) which generalizes (Fig. 1C)

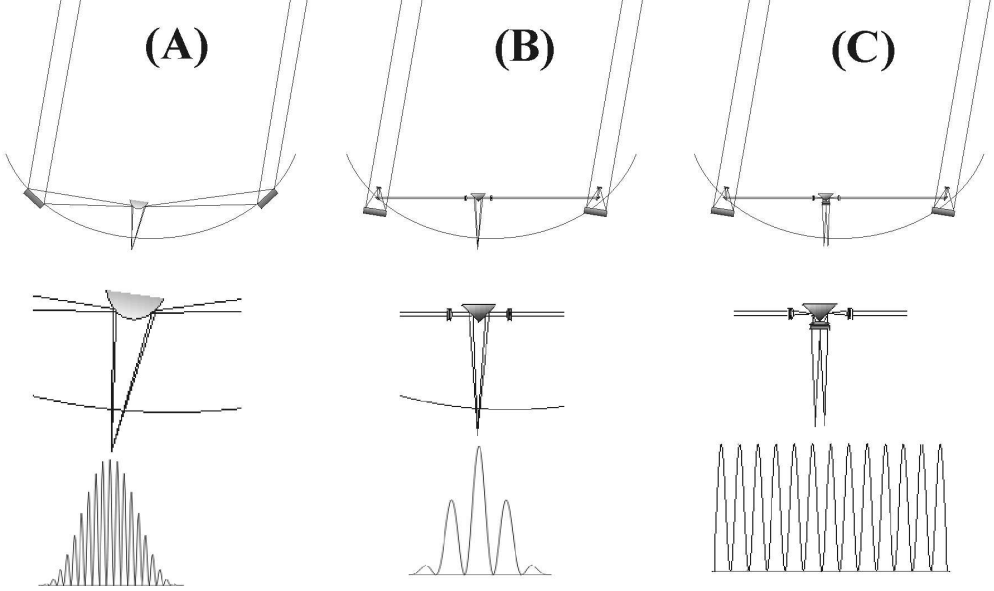

Fig. 1. Optical scheme of IRAN combinator with two telescopes. (A) and (B) the classical Fizeau versus Michelson beam-combinations, (C) instead of superimposing the Airy patterns from the telesopes it is possible to use a relay lens after the beam-combiner so as to stack the output pupils on the top of each other with a modulation depending on the output Airy discs distance.

set-up versus a fiber optics (F.O.) beam combiner (Mariotti et al., 1996) with the bonus of modal filtering and a moderately simplified beam-combiner. In the case of F.O. combination, the field of view would be limited to the Airy angular size of individual telescopes.

2.2. Intensity distribution for an on axis point-source

For sake of simplicity we consider a flat array of optical telescopes spread over co-centric circles with increasing radii and number of telescopes per circle. The telescopes afocal beams feed a central beam-combiner (Fig. 1C) after the constantly changing optical paths between the telescopes are corrected by optical delay lines for the sideral motion of the object. Note that the projected interference pattern at the focal plane of the interferometer will also change due to the sideral motion. This will correspond to an anamorphic change of the object brightness spatial sampling in the zenithal direction but its exact treatment is beyond the scope of the present study and will be adressed in a next paper.

2.2.1. Expression of the monochromatic intensity distribution for a point-source

Let $\boldsymbol{R}_i$ the positions of the N telescopes on the ground. These telescopes are supposed identical, with diameter d_0 and focal length f_0. Each telescope produces an Airy pattern of diameter $2.44\lambda f_0/d_0$ in its focal plane. We suppose that the incoming light is monochromatic with a wavelength of λ.

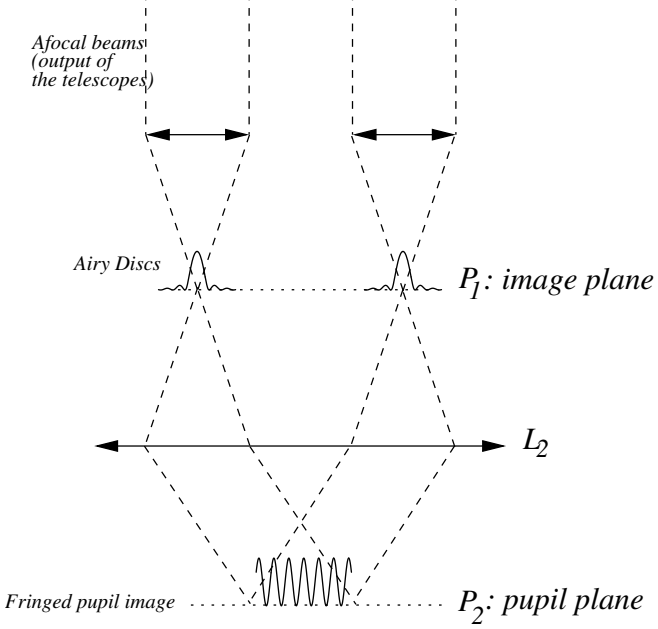

Fig. 2. Optical layout of the IRAN combinator. Afocal beams coming from the telescopes are focused on the image plane P_1 where several Airy spots are observed. A common lens L_2 produces a fringed pupil image in the pupil plane P_2.

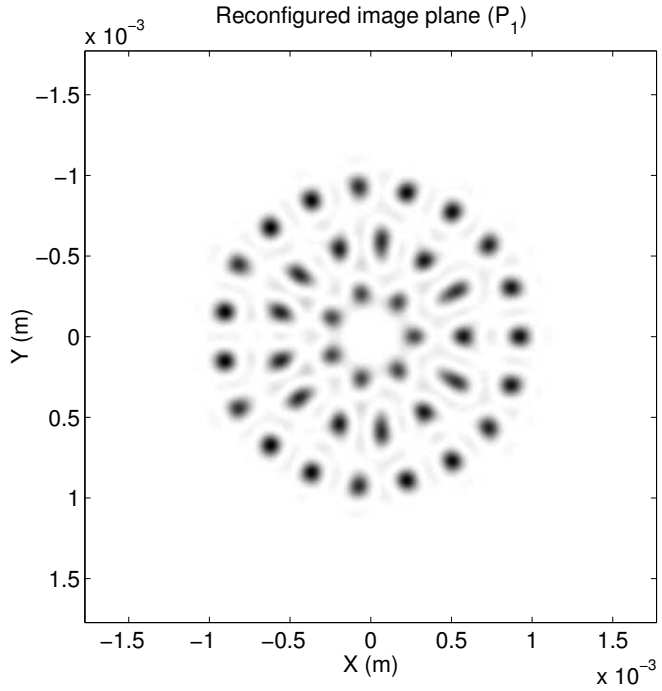

Fig. 3. Simulation of the configuration of the Airy discs in the plane P_1 for a interferometer with $N = 39$ telescopes (gray-level plot of the intensity). Experimental setup is described in the text. The units on both axii are in meter in the focal plane P_1. As the individual discs are coherent each other, their may interferate if they are too close. This is not a problem for the final image in the pupil plane; however that may affect the shape of the individual Airy patterns in the plane P_1 (giving the impression that the telecopes are different).

Beam-collection from the N telescopes of the array is done after N field-lenses (individual diameter d_1 and focal length f_1) will form corresponding Airy patterns on the N reflecting faces of a pyramidal beam combiner or by feeding bundled F.O. The collected — and not the combined — images in the common plane P_1 are centered at positions $\boldsymbol{\rho}_i$. The geometry of these images replicates the input telescope pupils orientation so that

$$\boldsymbol{R}_i = \gamma\ \boldsymbol{\rho}_i \tag{1}$$

where γ if the scaling factor between the two planes of input pupils versus output Airy discs. To fix further ideas, we chose a telescope configuration distributed over 3 circles of diameters D_1, $D_2 = 2.4D_1$ and $D_3 = 3.8D_1$. 7 telescopes are equally distributed on the first circle, 13 on the second one and 19 on the third one. This configuration is non-redondant in order to minimize the energy spread in the secondary peaks of the intensity pattern. All the figures shown in this paper, except section 4 about coronography corresponds to numerical simulations made with this configuration.

- Wavelength $\lambda = 10\mu$m
- Diameter of the telescope circles : $D_1 = 20$ m, $D_2 = 48$ m, $D_3 = 76$ m.
- $d_1 = 1$ cm, $f_1 = 10$ cm, no fiber optics are used for afocal beam transportation
- the Airy discs are spread over 3 circular circles of radii $r_1 = 1$, $r_2 = 2.4$ and $r_3 = 3.8$ in units of $2.44\lambda f_1/d_1$. This gives $\gamma = 4.1\,10^4$

The complex amplitude of the light in the plane P_1 is given by

$$\psi_1(\boldsymbol{\rho}) = A(\boldsymbol{\rho})\ *\ \sum_{i=1}^{N} \delta(\boldsymbol{\rho} - \boldsymbol{\rho}_i) \tag{2}$$

where $\boldsymbol{\rho}$ is the position vector in the plane and $\delta()$ is the Dirac delta distribution. $A(\boldsymbol{\rho})$ is the amplitude distribution of the images given by the lenses focusing each afocal beam. $A(\boldsymbol{\rho})$ is an Airy disc of diameter $2.44\lambda f_1/d_1$ if the light is transported by classical optics (mirrors) from the main telescope focus. In case of use of optical fibers, $A(\boldsymbol{\rho})$ is rather a Gaussian function.

Figure 3 shows a plot of the intensity distribution in the plane P_1 for our experimental setup.

A lens L_2 of diameter d_2 and focal length f_2 is placed after P_1 and produces in its focal plane P_2 a pupil image containing the interferences between the N beams. The amplitude in the plane P_2 is given by a Fourier transform of ψ_1 (Goodman, 1996) :

$$\psi_2(\boldsymbol{r}) = P(\boldsymbol{r})\ .\ \sum_{i=1}^{N} \exp -\frac{2i\pi \boldsymbol{r}.\boldsymbol{\rho}_i}{\lambda f_2} \tag{3}$$

where $P(\boldsymbol{r})$ is the Fourier transform of $A(\boldsymbol{\rho})$ (in the case of bulk optics $P(\boldsymbol{r})$ is the reimaged telescope pupil). The corresponding intensity is

$$I_2(\boldsymbol{r}) = |P(\boldsymbol{r})|^2\ .\ \left|\sum_{i=1}^{N} \exp -\frac{2i\pi \boldsymbol{r}.\boldsymbol{\rho}_i}{\lambda f_2}\right|^2 \tag{4}$$

2.2.2. Description of the intensity pattern and of the field of view

The function $|P(\boldsymbol{r})|^2$ is the achromatic pupil function. As for $A(\boldsymbol{\rho})$, its shape depends on the instrumental setup (bulky optics or optical fiber). It is ideally a uniform disc of diameter $d_1 f_2/f_1$. This function will delimit the field of view (FOV) of the interferometer[1] . The other term, denoted as

$$I_0(\boldsymbol{r}) = \left| \sum_{i=1}^{N} \exp -\frac{2i\pi \boldsymbol{r}.\boldsymbol{\rho}_i}{\lambda f_2} \right|^2 \tag{5}$$

is a complicated interference pattern which exhibits a pseudo Airy disc at the center with several rings. Figure 4 shows a simulation of the intensity distribution of this figure in the plane P_2 for the experimental configuration described above. A radial profile taken along the x-axis is displayed on Figure 5. It can be seen that the size of the central spot is that of an Airy disc corresponding to an aperture size D_3. Therefore the angular resolution R of the interferometer is conserved by the IRAN beam combination

$$R \simeq \frac{\lambda}{D_3} \tag{6}$$

Four our simulation that corresponds to a resolution $R = 0.027$ arcsec.

It can also be seen on Fig. 4 that the intendity pattern corresponding to our simulation exhibits a strong speckle-like noise starting at some distance from the central spot. This noise is due to the lack of filling in the plane P_1 and becomes noticeable at an angular distance of λ/D_1 from the center (see Figure 5). This is the angular resolution of a telescope of diameter D_1.

Therefore the intensity distribution, in our experimental setup, appears to be "clean" within a FOV equals to Airy disc of a telescope of diameter D_1, e.g. 0.12 arcsec four our simulation. In this clean zone, we observe secondary rings of amplitude of the order of 1/100 of the maximum. We can define a *clean FOV* of radius

$$F_c \simeq \frac{\lambda}{D_1} \tag{7}$$

in which direct imagery is possible with contrast conditions comparable with that of a monolithic telescope.

The total FOV of the interferometer is given by the function $|P(\boldsymbol{r})|^2$. In the ideal case where this pupil function equals to 1 within a circular area of diameter d_1 (diameter of the afocal beams) the function $|P(\boldsymbol{r})|^2$ is a uniform disc of diameter $d_1 f_2/f_1$. Making use of eq. 17, this can be converted into arcsec and gives a total FOV of value

$$F_t = \frac{d_1}{\gamma f_1} \tag{8}$$

[1] This is a consequence of the existence of an object-image convolution relation demonstrated in §2.4, allowing to convert a position in the focal plane into an angle on the sky. Therefore the spatial extension of the intensity distribution delimits a field of view.

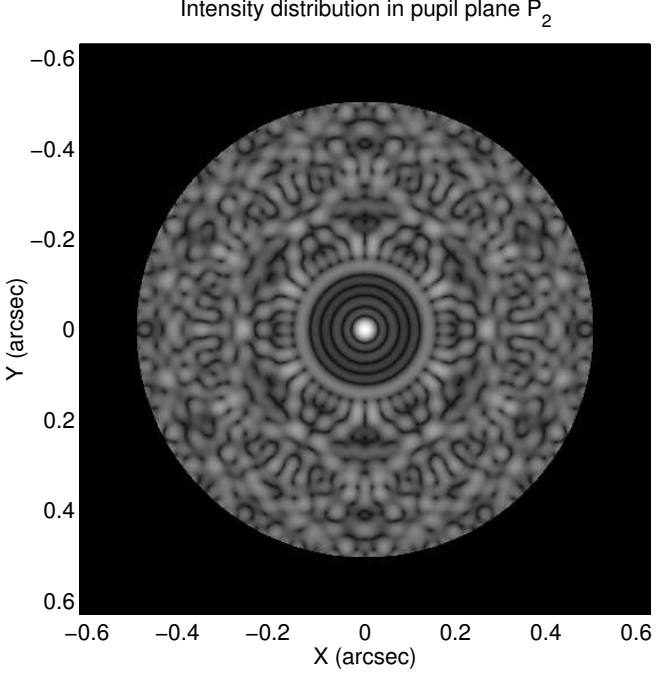

Fig. 4. Simulation of the intensity pattern $I_2(\boldsymbol{r})$ in the pupil plane P_2 for a interferometer with $N = 39$ telescopes observing an on-axis point-source. The wavelength is $\lambda = 10\,\mu$m. Experimental configuration is described in the text. A pseudo Airy disc is visible at the center. Axis units have been converted into arcsec according to eq. 17

In this ideal case the FOV depends only on the scaling factor γ and the aperture ratio of the lenses at the output of the fibers. For our example we have a total FOV of 0.5 arcsec. It can be theoretically as wide as wanted. In the case of a fiber-optics setup, the shape of the function $|P(\boldsymbol{r})|^2$ will be a gaussian function of width determined by the numerical aperture of the fiber (Ruilier, 1999).

2.2.3. Effect of a finite bandwith

The point-source intensity expression $I_2(\boldsymbol{r})$ is given in Eq. 4. It is the product of tho terms. One of them is achromatic ($|P(\boldsymbol{r})|^2$), the over being λ-dependent. Figure 6 displays the graph of $I_2(r)$ for three values of λ. It can been seen that the total FOV given by the width of $|P(\boldsymbol{r})|^2$ is independent of λ. Inside this FOV the structures are scaled proportionnaly to the wavelength.

For a finite bandwith $\Delta\lambda$ the intensity in the plane P_2 for an on-axis point-source will express as an integral over the wavelength λ

$$I_{\Delta\lambda}(\boldsymbol{r}) = \int_{\Delta\lambda} f(\lambda)\; I_2(\boldsymbol{r};\lambda)\; d\lambda$$

where $f(\lambda)$ is the product of the spectrum of the incident light by the spectral transmission of the experiment. Figure 7 displays the intensity pattern $I_{\Delta\lambda}(\boldsymbol{r})$ for a central wavelength $\lambda_0 = 10\mu$m anddifferent values of $\Delta\lambda$. The function $f(\lambda)$ has been taken to

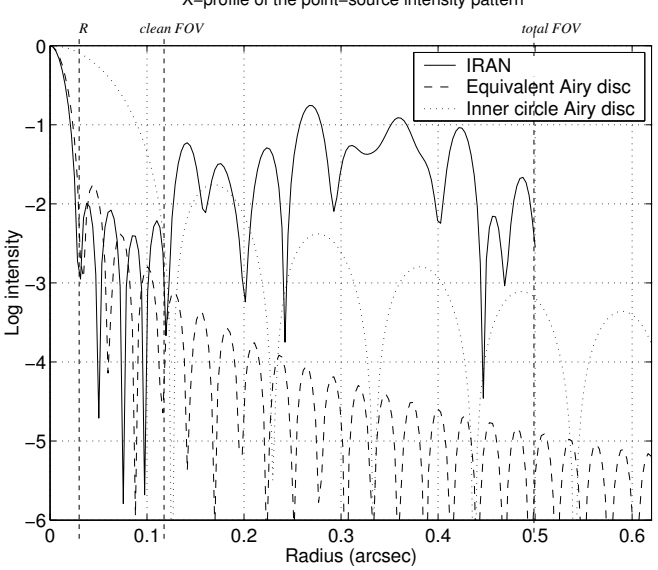

Fig. 5. Radial profile of the monochromatic point-source intensity distribution in the pupil plane P_2 Experimental configuration is described in the text. This profile is compared to the Airy disc of two monolithic telescopes: dashed line is for an aperture diameter D_3 (the outer circle of telescopes), dotted line is for an aperture diameter D_1 (inner circles of telescopes). Vertical dashed lines give the interferometer resolution R, the clean FOV and the total FOV.

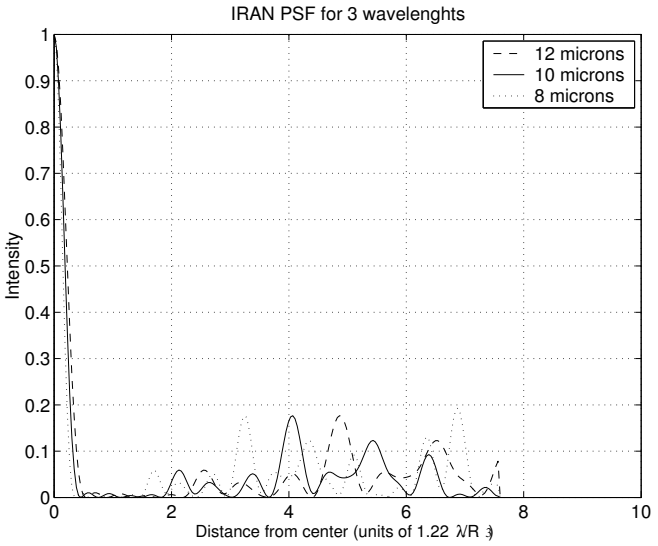

Fig. 6. Radial profile of the intensity point-source intensity distribution for tree different wavelengths, taken along the x-axis. Parameters of the simulation are described in the text. x-axis has been labelled in units of $1.22\lambda_0/D_3$, i.e. the angular resolution of the interferometer at $\lambda_0 = 10\mu$m.

unity. It appears that the speckle-like structures disperse as little spectra and that their contrast tends towards zero as the bandwidth increases.

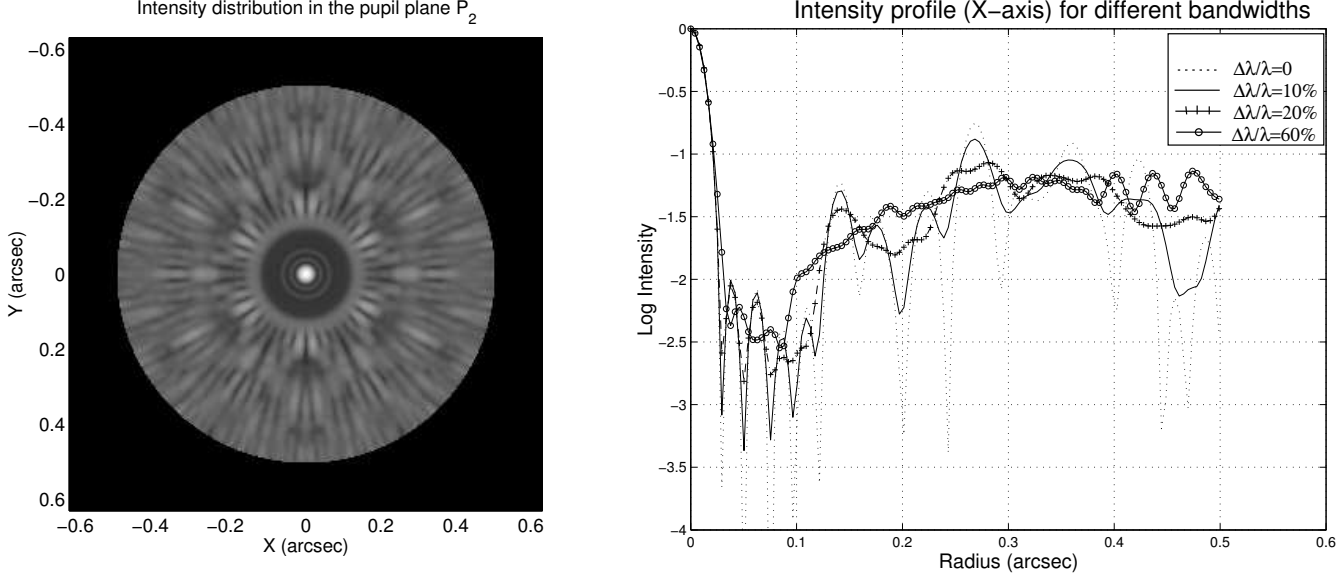

Fig. 7. Left : gray-level plot of the intensity distribution (point-source) for a central wavelength of 10μ m and an bandwidth $\Delta\lambda = 2\mu$m. Right : radial profile taken along the x-axis for different bandwidths.

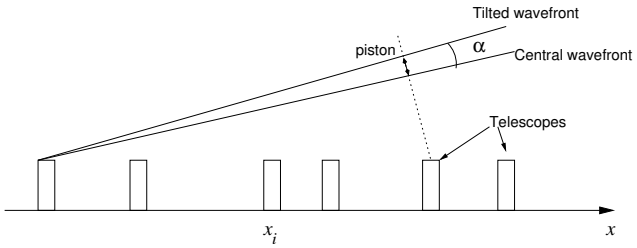

Fig. 8. Observation of an off-axis point-source at a distance α from the center of the field of view. On this one-dimensionnal configuration, each telescope is at a position x_i. The corresponding complex amplitude is multiplied by a piston term $\exp 2i\pi\alpha x_i/\lambda$.

2.3. Off axis point-source

We observe an off-axis point source in the direction given by the vector $\boldsymbol{\theta} = (\alpha, \delta)$ where α (resp. δ is the offset in right ascension (resp. declination). The images at the focus of each telescope are then shifted by a vector $\boldsymbol{\Delta} = f_0\boldsymbol{\theta}$. We assume that the angle between the axis and the source is small so that the shift $|\boldsymbol{\Delta}|$ is small compared to the size of the Airy disc. If the light is collected by an optical fiber, there is an attenuation factor on the complex amplitude denoted as $g(\boldsymbol{\theta})$.

The difference with the on-axis configuration is a piston term depending on the telescopes position

$$p_i = \exp \frac{2i\pi\boldsymbol{\theta}.\boldsymbol{R}_i}{\lambda} \tag{9}$$

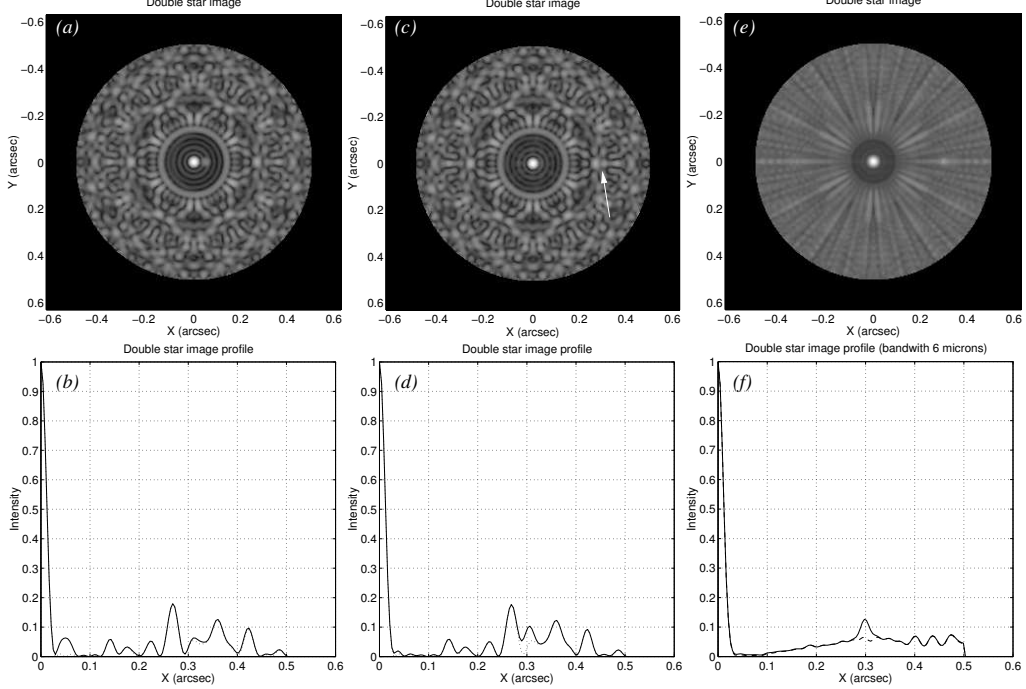

Fig. 9. Simulation of direct image of binary systems in the pupil plane P_2. The instrumental configuration is described in the text. Interferometer resolution is 30 mas. (a) monochromatic image of binary star of separation 50 mas, 3 magnitudes difference at a wavelength of 10 μm. (b) intensity profiles of the PSF (dashed line) and of the binary image (solid line), taken along the x-axis. (c) monochromatic image ($\lambda = 10\mu$m) of binary star of separation 300 mas, 3 magnitudes difference. The companion is at the arrow edge. (d) corresponding intensity profile (solid line) and PSF (dotted line). (e) polychromatic image ($\lambda = 10\mu$m, $\Delta\lambda/\lambda = 60\%$) of a binary of separation 300 mas and 3 mag difference. (f) intensity profiles of the corresponding image (solid line) and the PSF (dashed line) taken along the x-axis.

This piston term in conserved after beam combination. The complex amplitude of the light in the image plane P_1 becomes

$$\psi_1(\boldsymbol{\rho}) = g(\boldsymbol{\theta})A(\boldsymbol{\rho}) \ * \ \sum_{i=1}^{N} p_i \, \delta(\boldsymbol{\rho} - \boldsymbol{\rho}_i) \tag{10}$$

and in the pupil plane P_2 :

$$\psi_2(\boldsymbol{r}) = g(\boldsymbol{\theta})P(\boldsymbol{r}) \, . \, \sum_{i=1}^{N} \exp - \frac{2i\pi \, (\boldsymbol{r} - \gamma f_2 \boldsymbol{\theta}) \, . \boldsymbol{\rho}_i}{\lambda f_2} \tag{11}$$

The corresponding intensity is

$$I_2(\boldsymbol{r}) = g(\boldsymbol{\theta})^2 |P(\boldsymbol{r})|^2 \, . \, I_0 \, (\boldsymbol{r} - \gamma f_2 \boldsymbol{\theta}) \tag{12}$$

As for the on-axis case, the term $|P(\boldsymbol{r})|^2$ is a geometrical limitation of the field in the pupil plane. Within this limitation, the function $I_2(\boldsymbol{r})$ appears to be almost invariant by translation, as long as $g(\boldsymbol{\theta})$ remains close to 1, e.g. for small values of $|\boldsymbol{\theta}|$.

2.4. Object-image relation

We condider now an object composed of M point-sources of intensities O_i and positions $\boldsymbol{\theta}_i$ around the center of the field of view. We assume $|\boldsymbol{\theta}_i|$ small so that the image at the telescopes focus is fully contained in the Airy disc. The above relations give the intensity in the pupil plane P_2 :

$$I_2(\boldsymbol{r}) = |P(\boldsymbol{r})|^2 \sum_{i=1}^{M} O_i \; g(\boldsymbol{\theta}_i)^2 \; I_0\left(\boldsymbol{r} - \gamma f_2 \boldsymbol{\theta}_i\right) \tag{13}$$

Finally we consider the general case of on object of brightness distribution $O(\boldsymbol{\theta})$. Making the assumption that the object is small enough to be fully contained in the Airy disc of the telescopes, the above relation generalizes into

$$I_2(\boldsymbol{r}) = |P(\boldsymbol{r})|^2 \iint O(\boldsymbol{\theta})\, d^2\theta \; g(\boldsymbol{\theta})^2 \; I_0\left(\boldsymbol{r} - \gamma f_2 \boldsymbol{\theta}\right) \tag{14}$$

We introduce here the function

$$O'(\boldsymbol{\theta}) = O(\boldsymbol{\theta}) g(\boldsymbol{\theta})^2 \tag{15}$$

that represents the brightness distribution of the object weighted by the acceptance function of the optical fiber. The intensity in the pupil plane expresses as

$$I_2(\boldsymbol{r}) = |P(\boldsymbol{r})|^2 \; I_0(\boldsymbol{r}) \; * \iint O'(\boldsymbol{\theta}) \; \delta\left(\boldsymbol{r} - \gamma f_2 \boldsymbol{\theta}\right) \; d^2\theta \tag{16}$$

and finally

$$I_2(\boldsymbol{r}) = \frac{1}{(\gamma f_2)^2} \; |P(\boldsymbol{r})|^2 \; \left[I_0(\boldsymbol{r}) \; * \; O'\left(\frac{\boldsymbol{r}}{\gamma f_2}\right) \right] \tag{17}$$

Inside the boundaries delimited by the pupil function $|P(\boldsymbol{r})|^2$, we find the classical convolution relation between the PSF and the object (multiplied by the acceptance function of the optical fiber) scaled by the factor γf_2. This factor allows to convert a position x in meters in the focal plane into an angle $\theta = x/(\gamma f_2)$ in radian on the sky.

3. Direct images of stellar companions

The object-image convolution relation of Eq. 17 is an interesting property for imagery at the interferometer resolution. In the simple case of a double star, focal image is the sum of two PFSs with an angular separation equal to the separation of the star and its companion separation times the magnification factor and weighted by their intensity ratio.

Figure 9ab shows a numerical simulation of a double star monochromatic image with an angular separation 50 mas and magnitude difference of 3 (the experimental setup for this simulation is the 3-circles configuration described in section 2.2 operating at the wavelength $\lambda = 10\mu$m.). The angular separation has been chosen so that the companion's image forms into the "clean zone" described in section 2.2 where the direct

detection is easier.

When the angular separation of the binary increases, the speckle noise can make the companion detection difficult, as illustrated by Fig. 9cd where the companion image forms into the dirty zone of the main star intensity pattern.

Eq. 17 shows that the companion image is at the same position in P_2 whatever the wavelength. Increasing the bandwidth can be a mean to gain contrast since the speckles disperse. Figure 9ef shows a numerical simulation of a binary star image with separation 300 mas, 3 magnitudes difference and a relative bandwidth $\Delta\lambda/\lambda = 60\%$.

4. Coronography

Detecting very faint companions around a star becomes an optical challenge with the increasing magnitude difference. For a ExPN such as 51 Pegb this difference is of the order of 7 in N-Band. Various coronographic techniques have been proposed (Soummer et al., 2003 and references therein) to reject the energy of the on-axis star. The Achromatic Interfero Coronograph (AIC) (Gay & Rabbia, 1996) appears as particularly suitable for ExPN detection with the IRAN interferometric configuration which operated in the pupil plane. Principle of the ACI is summarized on Fig. 10. A lens L_3 is placed after the pupil plane P_2 and forms a geometric image of the image plane in P_1'. A classical laboratory Michelson interferometer is placed between L_3 and P_1'. A lens plus cat's eye optical system is introduced into one of the arms of this interferometer to produce a π dephasing and 180° rotation of the beam. In P_1' a total extinction of the light coming from an on-axis source is observed if the complex amplitude in P_1 is a pair function, i.e. for a symmetric telescope configuration. A lens L_4 focuses the light on the coronographied pupil plane P_2'. For an off-axis point-source, twin images are observed.

A numerical simulation has been performed in monochromatic light with a symmetric telescope configuration composed of 36 apertures spread over 3 circles (as in the previous section). We put 6 equally-spaced telescopes on the first circle, 12 on the second and 18 on the outer one. The external diameter is 76 m, the wavelength is 10 μm. Corresponding image plane P_1 displays a set of 36 Airy discs with the same geometry: in particular the complex amplitude is a pair function. Observed PSF with and without coronography are compared in Fig. 11 for an on-axis source. Extinction appears to be total at the computer precision level.

Double star simulations are shown in Fig. 12 for two different separations of the couple: a very small one (10 mas, interferometer resolution is 30 mas) and a large one of 200 mas (image of the companion is within the "dirty" zone of the main star's image). In each case the companion is easily detected. Magnitude difference was 5 in that simulation, but since the main star is fully extincted one can detect ExPNs with any magnitude

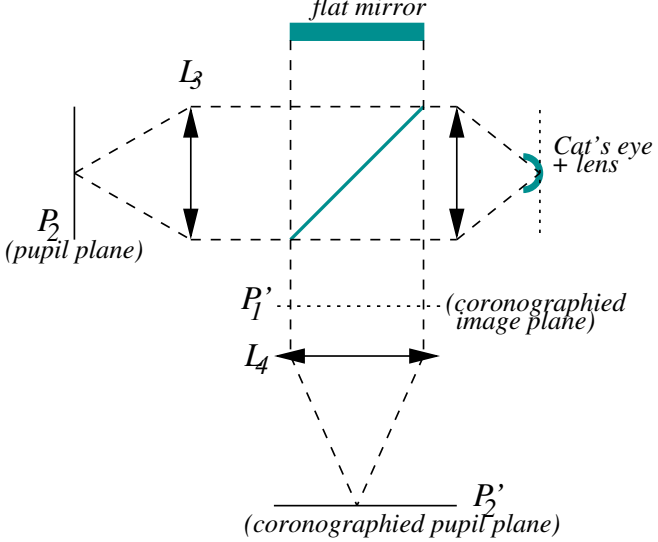

Fig. 10. Optical scheme of the AIC.

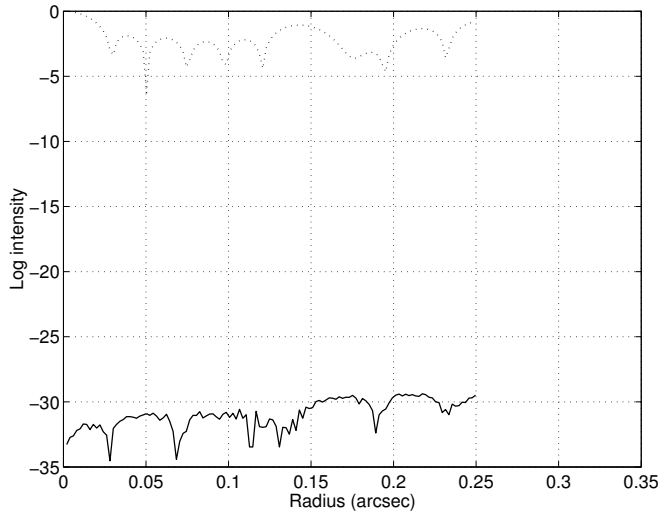

Fig. 11. Effect of the coronography on the intensity of an on-axis star. Dotted line: intensity profile (taken along the x-axis) in the pupil plane P_2 without coronography. Full line: the same in the plane P_2' after passage through the AIC.

difference. Technical and atmospherical constraints will be the only limitation of actual systems. A study of the AIC performances can be found in Baudoz et. al (2000a, 2000b). The details of the IRAN to AIC coupling need to be studied but are beyond the scope of the present paper.

5. Discussion

Optical aperture synthesis in optical wavelengths can reasonably be considered as a mature observing technique. Its effective application to detect exo-planetary systems or to image extended sources with high contrast still requires a number of conceptual and technological difficulties to be overcome. The IRAN concept developed in this paper gives to

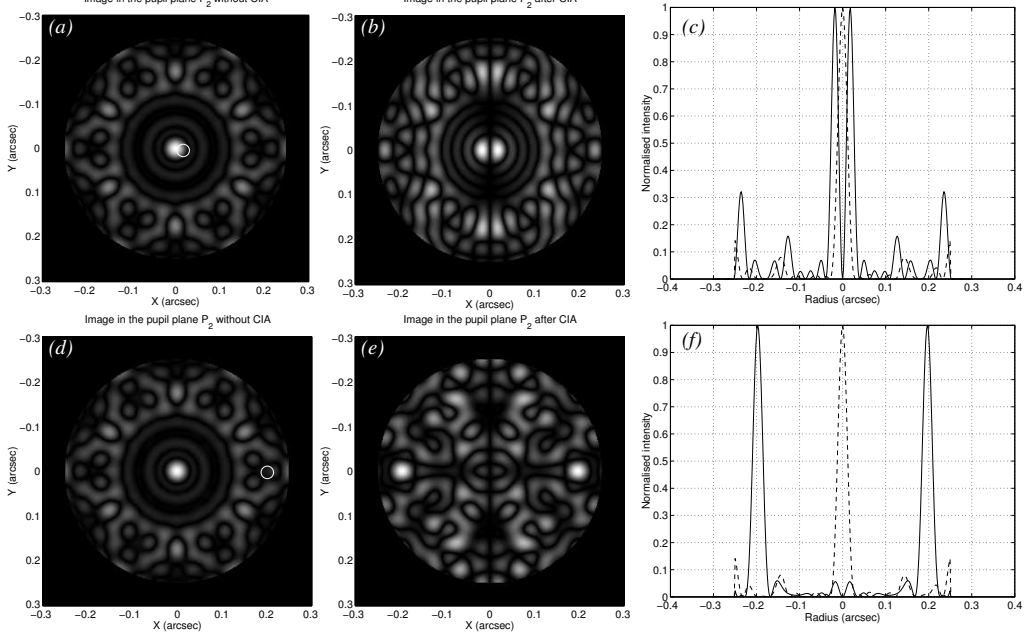

Fig. 12. Simulation of double stars monochromatic images ($\lambda = 10\mu$m) in the pupil plane with and without coronography. (a) gray-level plot of the intensity without AIC for a magnitude difference of 5 and a separation of 10 mas. The companion (not visible) is outlined by the white circle. (b) the same with AIC. (c) intensity profiles along the x-axis (solid line is with AIC, dotted line is without, maximum scaled to 1 for both curves). (d), (e) and (f) are the same plots for a separation of 200 mas.

our knowledge the first formal description and generic set-ups to fulfill this goal. The advantage of using a diluted array over a large monolithic mirror, if the input configuration of the telescopes were possible, is that the angular resolution of the interferometric array could be adaptively changed to match the angular separation of a star and its companion. A Fizeau-type is not however optimum in terms of sensitivity because the coherent energy dilutes among more and more fringes with expanding baselines. The alternative pairwise beam-combination is on the other hand inefficient when a very large number of sub-apertures where to be recombined. All-in-one combination of a large number of sub-pupils using IRAN approach is attractive because the coherent energy concentrates in almost one pixel. Since the convolution relation subsists across the output stacked pupil any extended object will produce a one-to-one image inside that pupil, also optimum in terms of read-out and background noise. The shortcoming of IRAN however is that for imaging applications only a small central "clean-field" can be straightforwardly used. Even in this case deconvolution techniques could be applied to get rid of side-lobe noise although half of the pupil would only be usable for the field of view.

We also suggested two generic beam-combinations: one using bulky optics, the second a F.O. beam-combiner. In the first case the field of view has a constant photometric field of view whilst in a F.O. combination this field is multiplied by the mono-mode F.O.

PSF. This does not hamper the imaging properties of IRAN but means that an ExPN for example would vanish photometrically with increasing distance from the center of the field. The F.O. combination is comparable with this respect to Labeyrie's densified pupil imaging where the field is modulated by the Airy figure of elementary telescopes.

The fact that IRAN produces a pseudo-Airy pattern inside the output stacked pupil arises the problem of central obscuration of the secondary mirror in a classical Cassegrain-coud set-up of the telescopes. Thus the central zone of IRAN's field of view is "blind" to the on axis component of the source which is imaged by the interferometer. Off-axis primary telescope mirror combinations would therefore be preferable to apply IRAN, a solution which is also desirable for thermal IR interferometry to minimize background optics emission.

It remains that our technique works only if the telescopes were co-phased. In a co-herenced array very probably the classical complex visibility using closure-phase and amplitude techniques are more applicable (Petrov et. al 2000, Lopez 2003). The question of array co-phasing can be adressed by various techniques using for instance another spectral region (Bely et al. 1997) or more recent algorithms using spatio-spectral properties of densified pupils (Pedretti & Labeyrie, 1999).

Finally as already mentioned the field of view of IRAN is limited to the Airy disc of individual telescopes. At 10μm wavelength for instance, this limitation does not appear drastic. Considering a 2m telescope for individual aperture, the Airy size is of the order of 1 arcsec. This size provides a field large enough to search for planets up to 100 AU distance from their parent star

6. Conclusion

We have presented a beam-combination technique with remarkable imaging properties for high dynamic imaging with diluted optical arrays. By construction the densified image and stacked-remapping technique from IRAN can be naturally combined with the Achromatic Interfero-Coronagraph (Gay & Rabbia, 1996), particularly suitable for coronographic imaging and detection of ExPNs compared to Labeyrie's densified pupil.

A number of questions remains open: the optimal beam combination, the effect of degrading co-phasing on the IRAN focal image, the imaging performances of IRAN after deconvolution for extended sources which exceed the central "clean-field" at the center of IRAN pupil and last but not least the formal definition of coronographic and/or nulling imaging of extended sources with IRAN. These question will be adressed in a next paper including a thorough comparison with the concept of DARWIN both in its nulling and imaging modes. The fore-coming studies and results will hopefully contribute to select the best beam-combination of next generation imaging optical arrays like the VLTI or extension of already opertaing imaging arrays like NPOI.

7. Acknowledgments

We are grateful to N. Minec and J. Gay for constructive discussions. L. Abe benefits from a CNES post-doctoral fellowship.

References

Baudoz P., Rabbia Y., Gay J., 2000a, A&AS 141, 319

Baudoz P., Rabbia Y., Gay J., Burg R., Petro L., Bely P., Fleury B., Madec P.-Y., Charbonnier F., 2000b, A&AS 145, 341

Beichman C., Coulter D., Lindensmith C. Lawson P., 2002, in "Future Research Direction and Visions for Astronomy", proc. SPIE 4835, 115

P.Y. Bely, C. Haniff, A.H. Greenaway, M. Lattanzi, R. Laurance, J. Noordam, F. Vakili, S. Volont, O. von der Luhe, 1997, in "Kilometric Space Interferometer", ESA-SP 96(97)

Bracewell R. N., 1978, Nature 274, 780

Chelli A., Mariotti J.-M. 1986, A&A, 157, 372C

Gay J., Rabbia Y., 1996, C.R. Acad. Sci. Paris, 322 Série IIb, 265

Gillet, S., Riaud, P., Lardire O., Dejonghe J., Schmitt J., Arnold L., Boccaletti A., Horville D., Labeyrie, A., 2003, A&A 400, 393

Gondoin P., Absil O., et al., 2003, in "Interferometry for Optical Astronomy II", proc. SPIE 4838, 700

Gonsalves R., Nisenson P., 2003, PASP 115, 706

Goodman J.W., 1996, Introduction to Fourier Optics, Mc Graw-Hill Science

Labeyrie A. Le Coroller H., Dejonghe J., Martinache F., Borkowski V., Lardiere O., Koechlin L., 2003, in "Interferometry in Space", proc. SPIE 4852, 236

Lopez, B., SF2A-2003, Bordeaux, France, June 16-20, 2003. Eds.: F. Combes, D. Barret and T. Contini. EdP-Sciences, Conference Series, p. 155.

Mariotti J.-M., Coudé du Foresto V., Perrin G., Zhao P., Léna P., 1996, A&AS. 116, 381

Mennesson B., Mariotti J.-M., 1997, Icarus 128, 202

Michelson A. A., 1920, ApJ 51, 257

Pedretti, E., Labeyrie, A., Astron. Astrophys. Suppl., v.137, p.543-551

Petrov R., Malbet F., et al., 2000, in "Interferometry in Optical Astronomy", proc SPIE 4006, 68

Rousselet-Perraut K., Mourard D., Vakili F., 1997, Optical Engineering 36, 980

Ruilier C., 1999, PhD. Thesis, Observatoire de Paris

Soummer R., Aime C. Falloon P. E., 2003, A&A 397, 1161

Tallon M., Tallon-Bosc I., 1992, A&A 253, 641